

Differential Path Considerations in Optical Stellar Interferometry

T. A. ten Brummelaar

Center for High Angular Resolution Astronomy, Georgia State University
Applied Optics **34**, 2214-2219, (1995)

Abstract

A formulation of the differential air path problem for a large baseline optical interferometer is presented. Since air is a dispersive medium, each wavelength will have a different optical path length. This can be corrected to a large extent by placing an extra piece of glass in each arm of the interferometer. The problem then becomes analogous to doublet achromat design where, in this case, the air path takes the place of one piece of glass. Atmospheric refraction and field of view considerations also amount to changing the differential paths within the interferometer. All three effects can therefore be considered to be aspects of the same problem. The focus of this work has been for the proposed array to be developed by the Center for High Angular Resolution Astronomy (CHARA Array), although the results are applicable to any optical array.

1 Introduction

Most optical arrays, either on the ground or in the planning stages, include large vacuum systems for their optical path length equalization (OPLE) systems. In the proposed Center for High Angular Resolution (CHARA) array[1, 2], which includes seven optical channels, the OPLEs are to be in a thermally controlled air environment. Unfortunately, large differential air paths can be created between beams resulting in dispersion and loss of coherence. This can be corrected by adding extra pieces of glass of appropriate thickness in each beam. This method is being used at the Observatoire de la Côte d'Azur on both the I2T[3] and the GI2T[4] and is also planned for use in the Sydney University Stellar Interferometer SUSI[5]. A formulation of the differential path problem, including atmospheric refraction and field of view, is presented below.

Let us assume that many narrow-band channels evenly distributed in wavenumber space are used to get the equivalent of a larger bandpass. This approach differs from the treatment of dispersion by Tango[6] who looks at the problem of a single, large-bandwidth, pixel. The calculations below are based largely on an internal report by Traub[7] for the Infra-Red Optical Telescope Array[8] (IOTA) project. The technical report on dispersion effects in the Navy Prototype Optical Interferometer (NPOI)[9] by Ling[10] was also consulted, although the solution proposed for NPOI-BOA (rotating glass plates) would not be suitable for CHARA as its air paths are much larger.

The basic results are that, whereas no correction is required in the IR band, in the visible band dispersion must be corrected through the use of approximately 0.43 mm of BK7 glass for every meter of differential air path. A second effect of the addition of glass to one arm is to move the fringes up to tens of centimeters away from the original white light position. This shift makes simultaneous observations in the visible and IR bands difficult if not impossible. However, if one is willing to forgo science measurements in the visible system and use that system only for fringe tracking without dispersion correction, it should then be possible to use the IR system for simultaneous imaging.

2 Geometry

Let us consider a single pair of telescopes with the geometry shown in figure 1. Two pairs of beams are shown in this diagram, one indicating the center of the imaging area determined by the tip/tilt servo at a true zenith angle of θ and a second beam pointing at a point of scientific interest, at an angle α away from this position. Both beams are then refracted by the atmosphere and reach the telescopes with an angular separation of β . This angle is magnified by the telescopes by a factor of M and sent through the interferometer optics. One arm passes through the OPLE whose length is x_{OPLE} , the rest of the internal paths are assumed to be identical. Both beams then pass through atmospheric refraction correctors (ARC) so that all beams are parallel to the first order. Finally, one arm passes through a longitudinal dispersion corrector (LDC) before the beams are combined to form fringes. In the calculations to follow we define two fixed wavelengths: the tracking wavelength λ_{track} is the wavelength used for the detector of the tip/tilt servo and defines the pointing position; the phasing wavelength λ_{ph} defines the wavelength used to track the fringes. The center of the imaged area, for which both tip/tilt and phase are tracked is normally referred to as the phase center.

In the CHARA array sections of vacuum pipe are used to introduce DC path correction whereas the OPLE carriage itself has a maximum optical length of only 100m. This has the equivalent effect of reducing the projected baseline. The maximum zenith angle planned for the array is 50° . Thus in most of the calculations that follow a baseline of 100m and zenith angle of 50° are used as worse case figures.

3 Atmospheric Refraction

The effect of atmospheric refraction is well understood and easily corrected with Risley prisms. The change in the zenith angle introduced by the atmosphere is

$$\Delta\theta = \left(\frac{1}{n_{\text{air}}(\lambda)} - 1 \right) \tan \theta. \quad (1)$$

Note that this expression is different from that normally cited because θ has been defined to be the true, rather than the observed, zenith angle. If the angular separation of the beam from the tracking center were α above the atmosphere, it would be

$$\beta(\lambda) = \frac{1}{n_{\text{air}}(\lambda)} (\tan \theta + \alpha) - \frac{1}{n_{\text{air}}(\lambda_{\text{track}})} \tan \theta \quad (2)$$

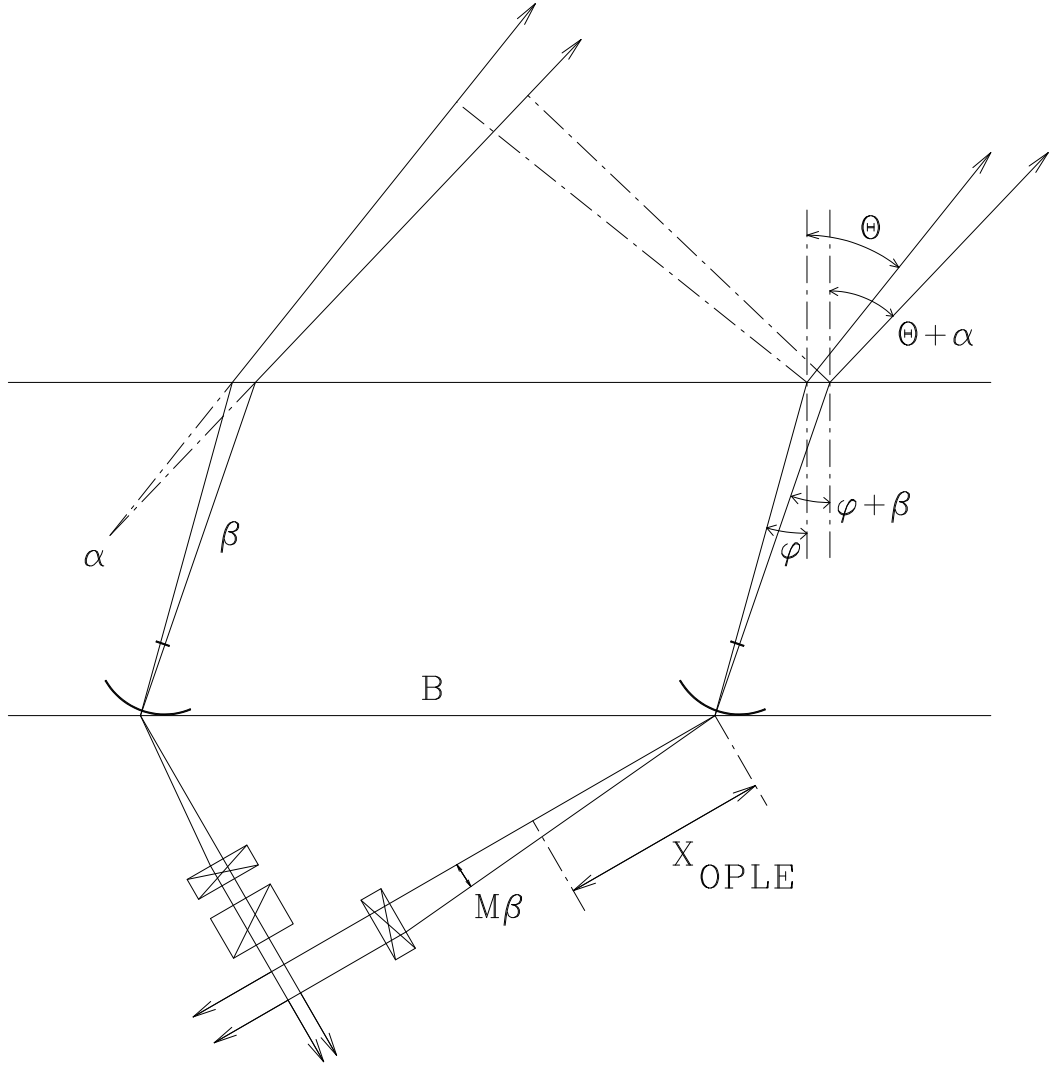


Figure 1: Diagram of the geometry used to calculate differential path effects: The telescopes (curved lines) are mounted on the ground (lower horizontal line) and separated by the baseline distance B . The upper horizontal line represents the top of the atmosphere. The ARC's (one in each beam) are represented by the rectangles with crossed lines, and the LDC by the rectangle with the single diagonal line. ϕ is the zenith angle of the scientific target after refraction by the atmosphere. The dashed-dotted line represent the baselines of the pointing center and center of scientific interest.

after it has been refracted by the atmosphere where terms of the order $\alpha(n_{\text{air}} - 1)$ are assumed to be small.

The difference in angle between the tracking center and the direction of observation has two effects and both are due entirely to the differential path of the two beams. The first effect is a differential optical path of $x_{\text{OPLE}}/\cos(M\beta(\lambda))$ between the two beams pointing at the position of scientific interest and is a second order effect that can be ignored in this analysis. For example, in the case of the CHARA array, $M = 8$, and we set $x_{\text{OPLE}} = 100$ m, $\alpha = 1''$, $\lambda_{\text{track}} = 0.4 \mu\text{m}$, $\lambda = 0.55 \mu\text{m}$ and $\theta = 50^\circ$, the difference in path length is $0.8 \mu\text{m}$. As the analysis that follows will show, this is much less than the size of the fringe envelope. The second effect is a beam displacement. With the numbers used above, this amounts to a beam displacement of 0.7 cm. In the case of the CHARA Array, which will employ beam reducing telescopes to further reduce the beam size after the OPLE's, a beam displacement of 1 mm results. The ARC then ensures that, although displaced, the beams are parallel to the optical axis. Thus, because lenses are being used to form images in all the detectors and as long as the size of the optics is chosen so that no beam masking occurs, this beam displacement has little or no effect on fringe formation. One may therefore conclude that atmospheric refraction is not a first-order problem for the CHARA array, and the ARC can be placed at the back end of the interferometer, as long as it is as close as possible to the beam reducing telescopes.

One can conclude then that atmospheric refraction can be largely ignored and that equation (2) can be approximated by

$$\beta(\lambda) = \frac{\alpha}{n_{\text{air}}(\lambda)}. \quad (3)$$

The analysis in Section 4 was repeated with the full expression shown in equation (2) and including OPLE path differences, to test this conclusion. The results did not differ significantly from those presented below.

4 Longitudinal Dispersion

The differential air path of the two beams in the interferometer results in different optical path lengths at different wavelengths. It is hoped that this difference can be corrected if a piece of glass is placed in the beam that has the shortest air path. Therefore, to the first order, one writes the optical path length difference (OPD) at a given wavelength between the two interfering beams as

$$\text{OPD} = \underbrace{B \sin(\theta + \alpha)}_{\text{Baseline Projection}} + \underbrace{n_{\text{glass}}(\lambda)d}_{\text{LDC}} - \underbrace{n_{\text{air}}(\lambda)x_{\text{OPLE}}}_{\text{OPLE}}. \quad (4)$$

Here d is the thickness of the glass in the LDC. The length of the OPLE can then be defined as a displacement l from the position x_0 ,

$$x_{\text{OPLE}} = x_0 + l \quad (5)$$

where x_0 is the OPLE position for zero path length difference when $d = l = \alpha = 0$ and at the wavelength defining the phase center λ_{ph} . Thus

$$x_0 = \frac{1}{n_{\text{air}}(\lambda_{\text{ph}})} B \sin \theta. \quad (6)$$

Because the field of view α is known to be small, one can expand the sine term in equation (4) and write the optical path length difference as

$$\text{OPD} = B \sin \theta \left(1 - \frac{n_{\text{air}}(\lambda)}{n_{\text{air}}(\lambda_{\text{ph}})} \right) + n_{\text{glass}}(\lambda)d - n_{\text{air}}(\lambda)l + \alpha B \cos \theta. \quad (7)$$

The detected fringe pattern at a single wavelength depends on this optical path length difference as follows

$$I(\nu) = 1 + V(\nu) \cos(2\pi\nu \text{OPD}), \quad (8)$$

where the wavenumber $\nu = \frac{1}{\lambda}$ has been used instead of the wavelength λ and $V(\nu)$ is the fringe visibility which is also a function of the wavenumber. This expression is integrated over a waveband centered on ν_0 and width $\Delta\nu$, which is assumed to be small, on each pixel of the detector, and therefore the detected fringe pattern in a single pixel is

$$\begin{aligned} F(\nu_0, \Delta\nu) &= \frac{1}{\Delta\nu} \int_{\nu_0 - \frac{\Delta\nu}{2}}^{\nu_0 + \frac{\Delta\nu}{2}} I(\nu) d\nu \\ &= 1 + \frac{V(\nu_0)}{\Delta\nu} \int_{\nu_0 - \frac{\Delta\nu}{2}}^{\nu_0 + \frac{\Delta\nu}{2}} \cos 2\pi H(\nu) d\nu \end{aligned} \quad (9)$$

where

$$H(\nu) = \nu \left[B \sin \theta \left(1 - \frac{n_{\text{air}}(\nu)}{n_{\text{air}}(\nu_{\text{ph}})} \right) + n_{\text{glass}}(\nu)d - n_{\text{air}}(\nu)l + \alpha B \cos \theta \right], \quad (10)$$

and where we assume that the visibility does not change substantially across the small bandpass $\Delta\nu$.

Because the bandpass of each detector channel is small, we can expand the refractive indices of air and glass around ν_0 so

$$\begin{aligned} H(\nu) &= \nu B \sin \theta \left(1 - \frac{n_{\text{air}}(\nu_0)}{n_{\text{air}}(\nu_{\text{ph}})} - \frac{n'_{\text{air}}(\nu_0)}{n_{\text{air}}(\nu_{\text{ph}})}(\nu - \nu_0) \right) \\ &\quad + d \left(n_{\text{glass}}(\nu_0) + n'_{\text{glass}}(\nu_0)(\nu - \nu_0) \right) \nu \\ &\quad - l \left(n_{\text{air}}(\nu_0) + n'_{\text{air}}(\nu_0)(\nu - \nu_0) \right) \nu + \alpha B \nu \cos \theta. \end{aligned} \quad (11)$$

Next we use the new variable $\eta = \nu - \nu_0$ and, after a bit of algebra, find that

$$H(\nu) = \mathcal{A} + \mathcal{B}\eta + O(\eta^2) \quad (12)$$

where

$$\mathcal{A} = \nu_0 B \sin \theta \left(1 - \frac{n_{\text{air}}(\nu_0)}{n_{\text{air}}(\nu_{\text{ph}})} \right) + \nu_0 n_{\text{glass}}(\nu_0)d - \nu_0 n_{\text{air}}(\nu_0)l + \nu_0 \alpha B \cos \theta \quad (13)$$

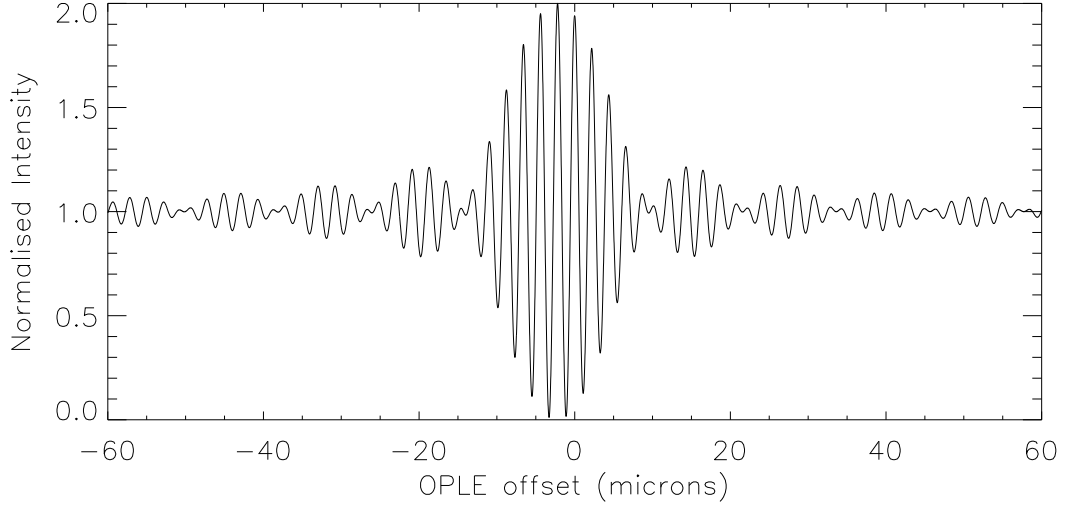


Figure 2: fringe pattern predicted for a bandpass of 2.0 to 2.4 μm , a phase center wavelength of 2.2 μm , a baseline of 8 meters and a zenith angle of 30 degrees.

and

$$\begin{aligned} \mathcal{B} = & -\nu_0 B \sin \theta \frac{n'_{\text{air}}(\nu_0)}{n_{\text{air}}(\nu_{\text{ph}})} + B \sin \theta \left(1 - \frac{n_{\text{air}}(\nu_0)}{n_{\text{air}}(\nu_{\text{ph}})} \right) \\ & + (\nu_0 n'_{\text{glass}}(\nu_0) + n_{\text{glass}}(\nu_0)) d - (\nu_0 n'_{\text{air}}(\nu_0) + n_{\text{air}}(\nu_0)) l + \alpha B \cos \theta. \end{aligned} \quad (14)$$

The detected signal in a single pixel as defined in equation (9) can then be calculated to yield

$$F(\nu_0, \Delta\nu) = 1 + V(\nu_0) \frac{\sin \mathcal{Z}}{\mathcal{Z}} \cos 2\pi \mathcal{A} \quad (15)$$

where

$$\mathcal{Z} = \Delta\nu \pi \mathcal{B}. \quad (16)$$

The resulting fringe pattern consists of two parts: an oscillating cosine term that represents the fringes themselves and a modulating a sinc function, the Fourier transform of the square bandpass. Had we used some other form for the bandpass, this sinc function would become the Fourier transform of the filter function chosen. For example, if we were to use a Gaussian function for the bandpass the fringe envelope would also be a Gaussian. An example of some fringes is given in figure 2. Furthermore, note that the maximum visibility is unity. Had we included the quadratic, or higher, terms in the expansion this would no longer be the case and the maximum visibility would be reduced.

It is clear from figure 2 that the fringe pattern envelope peak is not at the OPLE zero point $l = 0$ but at a position where $\mathcal{Z} = 0$. This occurs when $l = l_0$ where

$$l_0 = \frac{B \sin \theta \left[1 - \frac{n_{\text{air}}(\nu_0)}{n_{\text{air}}(\nu_{\text{ph}})} - \nu_0 \frac{n'_{\text{air}}(\nu_0)}{n_{\text{air}}(\nu_{\text{ph}})} \right] + (\nu_0 n'_{\text{glass}}(\nu_0) + n_{\text{glass}}(\nu_0)) d + \alpha B \cos \theta}{\nu_0 n'_{\text{air}}(\nu_0) + n_{\text{air}}(\nu_0)}. \quad (17)$$

The enumerator contains three terms. The first represents the projected baseline $B \sin \theta$ and is the only term that depends on $n_{\text{air}}(\nu_{\text{ph}})$ which, unless the phasing wavenumber is very different from the band of scientific interest, can be set to unity to leave only the refractive index of the air and its derivative multiplied by the central wavenumber. The second term represents the effect of the dispersion corrector glass and once again contains a refractive index and its derivative multiplied by the wavenumber. The third term in the enumerator represents the effective change in the projected baseline that is due to an expanding field of view. The effect of this term is discussed in section 6. The denominator, as is shown below, represents the width of the coherence envelope and once again involves a refractive index and its derivative multiplied by the wavenumber. To consider larger bandpasses in each pixel one would require the second order properties of the refractive indices.

The fringe envelope reaches its first minimum when $\mathcal{Z} = \pm\pi$. The width of the fringe envelope is therefore

$$\Delta l = \frac{\pm 1}{\Delta\nu} \times \frac{1}{\nu_0 n'_{\text{air}} + n_{\text{air}}(\nu_0)} \quad (18)$$

and if one notes that $n_{\text{air}} - 1 \ll 1$ and that typically $\nu n'_{\text{air}}(\nu)$ is of order $n - 1$ it can be shown that the fringe envelope only depends on the bandwidth in wavenumber, that is

$$\Delta l = \frac{\pm 1}{\Delta\nu} \quad (19)$$

which is equivalent to the common expression of $\lambda^2/\Delta\lambda$ for the coherence length.

Thus one sees that the fringe envelope center moves away from the OPLE zero point and that this distance from the OPLE center depends on the baseline, the zenith angle, the field of view angle, the amount of glass used in the LDC, and the wavelength. Figure 3 shows the position of the fringe envelope for a baseline of 100 meters, a zenith angle of 50° , no glass in the LDC, and a range of 128 pixels spaced over the bandpass of 0.6 to 0.8 μm . This plot makes it clear that longitudinal dispersion correctors are required. Only a small range of pixels lies within the 5% loss range of the curve for any given OPLE position.

The addition of glass to one arm should make it possible to ensure that all the bands have a central fringe position l_0 that is well within the fringe envelope size Δl . To calculate how much glass is required, let us force the two outermost bandpasses to have the same fringe positions. Noting that the denominator in equation (17) depends upon only the envelope width and is therefore relatively constant for all pixels and that the refractive index of air at the phasing wavelength will be very close to unity we find that the required amount of glass is

$$d = B \sin \theta \frac{n_{\text{air}}(\nu_1) - n_{\text{air}}(\nu_2) + \nu_1 n'_{\text{air}}(\nu_1) - \nu_2 n'_{\text{air}}(\nu_2)}{n_{\text{glass}}(\nu_1) - n_{\text{glass}}(\nu_2) + \nu_1 n'_{\text{glass}}(\nu_1) - \nu_2 n'_{\text{glass}}(\nu_2)} \quad (20)$$

where ν_1 and ν_2 are the central wavenumbers of the two outermost bandpasses to be used. So, for example, if the projected baseline is 1 m with the bandpass 0.6-0.8 microns the dispersion of the air-path can be compensated by adding 0.43mm of BK7 glass to one arm of the interferometer. This result can be compared with the results of the use if 0.51mm of fused silica that were given given by Tango. The results differ not only in the type of glass used but also in the difference in optimization criteria. In our case we are trying to ensure that two narrow and widely separated bands have an identical fringe location. The

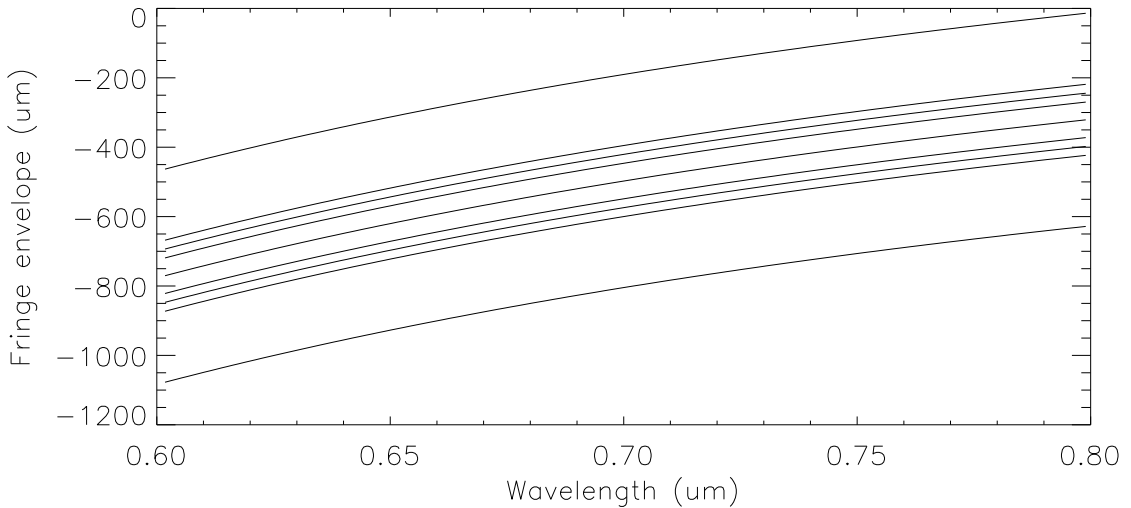


Figure 3: The fringe envelope for a baseline of 100 m and a zenith angle of 50° without dispersion correction. The central line represents the center of the envelope. The succeeding pairs of lines represent, respectively, the 95% point, the 90% point, and the 85% point. The outermost lines represent the first zero.

analysis of Tango, on the other hand, focuses on the minimization of the residual dispersion in a single wide-band channel.

Let us demonstrate the effectiveness of this single glass solution by performing the same calculations as were performed for figure 3 except that 3.3 cm of glass, as determined by equation (20), have been added in to the LDC. The results are plotted in figure 4. Now that this extra glass has been inserted, the entire bandpass is contained within the 5% loss lines, indeed an even bigger bandpass could be corrected. Note, however, that the positions of the fringes have been moved some 5.2 cm. This shift of the fringe maximum is due to the phase changes imposed by the corrector plate on one beam and can be calculated by means of

$$l(d) = d \times \frac{\nu_0 n'_{\text{glass}}(\nu_0) + n_{\text{glass}}(\nu_0)}{\nu_0 n'_{\text{air}}(\nu_0) + n_{\text{air}}(\nu_0)}. \quad (21)$$

5 Infrared Band

With equations (17) and (18), it is easy to generate similar plots for the IR band. For example, figure 5 shows the fringe envelope for an IR band of 20 pixels that covers 2-2.5 μm , once again with a baseline of 100 m, a zenith angle of 50° and no glass in the LDC. Fortunately, because the refractive index of air changes slowly in this band, no dispersion correction is required for the IR. Similar calculations can show that this is also the case for the angular change introduced by atmospheric refraction. Unfortunately, since both an ARC and an LDC are required for the visible band, the effect of which is to move the fringes several centimeters, it is unlikely that it will be possible to observe simultaneously in both

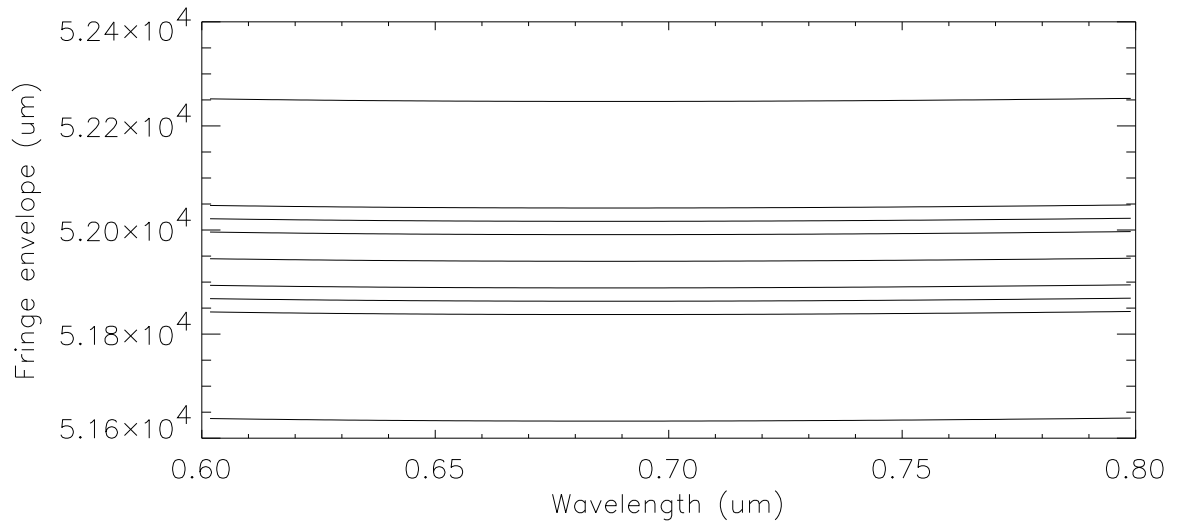


Figure 4: The fringe envelope for a baseline of 100 m and a zenith angle of 50° with dispersion correction. The central line represents the center of the envelope, and the successive liens are as for Fig 3.

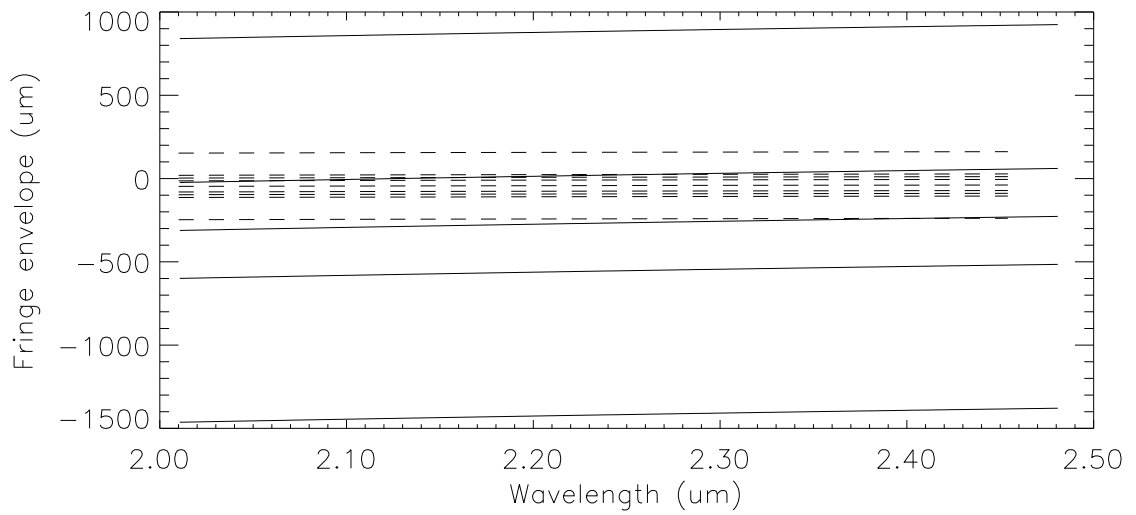


Figure 5: The IR fringe envelope (solid lines) for a baseline of 100 m and a zenith angle of 50 degrees without dispersion correction. The fringes for a visible band of $0.9\text{-}1.0 \mu\text{m}$ for the same situation and no dispersion correction are represented by dashed lines. Note that even without dispersion correction, the IR fringes lie completely within the range of the visible fringes.

bands. It may be possible to use both bands simultaneously if separate dispersion correctors are used for each band, however, this would add significantly to the cost and complexity of the instrument.

If one were willing to forgo using the visible system for visibility measurements and to use it only for fringe tracking, this problem would be solved by simply removing the LDC altogether. For example, in figure 5, superimposed on the IR fringe envelope lines are dashed and dotted lines representing the positions of the visible fringes in the band $0.9 - 1.0 \mu\text{m}$ where dispersion correction has not been used. The IR fringes lie almost completely within the 10% loss area of the visible fringes. It should therefore be possible to offset track if one uses the $0.9 - 1.0 \mu\text{m}$ band while imaging in the IR band. This scheme also works at other visible bands although increased visibility losses occur.

6 Field of View

From equation (17) we see that the contribution to fringe displacement that is due to changing the field of view angle α is

$$l_{\text{FOV}} = \frac{\alpha B \cos \theta}{\nu_0 n'_{\text{air}}(\nu_0) + n_{\text{air}}(\nu_0)}. \quad (22)$$

If we say that we are permitted to go to some fraction F of the total fringe envelope, then we can write

$$l_{\text{FOV}} = 2F\Delta l \quad (23)$$

which, after solving for α gives

$$\alpha = \frac{2F}{\Delta\nu B \cos \theta} \quad (24)$$

from which we can calculate the usable field of view for the array. We must also remember that if the two Airy patterns created by the beams that correspond to the tracking center do not overlap, no fringes are seen at all. This is because, in almost all situations, the tip/tilt tracking object is also the scientific target and the area of scientific interest will be smaller than the resolution limit of the individual telescopes. This gives us an absolute maximum field of view of $\frac{2.4\lambda}{D}$ where for the CHARA Array the diameter $D = 1 \text{ m}$. If the detector pixels are evenly distributed in wavenumber space the field of view in a given band depends only on the pixel size in wavenumber and the projected baseline. Two examples are given in figure 6, one for the 20 pixel IR band from 2.0 to $2.5 \mu\text{m}$ and the other for the 128 pixel visible band from 0.6 to $0.8 \mu\text{m}$. The fraction of coherence loss for the IR band was 50% whereas that of the visible was 5%.

7 Conclusion

This analysis has shown that dispersion can be corrected to a large extent by a single piece of BK7 glass. Atmospheric refraction was shown to be a second-order effect that can be corrected if one uses Risley prisms at the back end of the interferometer. For the IR band neither an ARC nor an LDC would be required, although the fringe displacement in the visible band that is caused by dispersion correction, it would probably make simultaneous

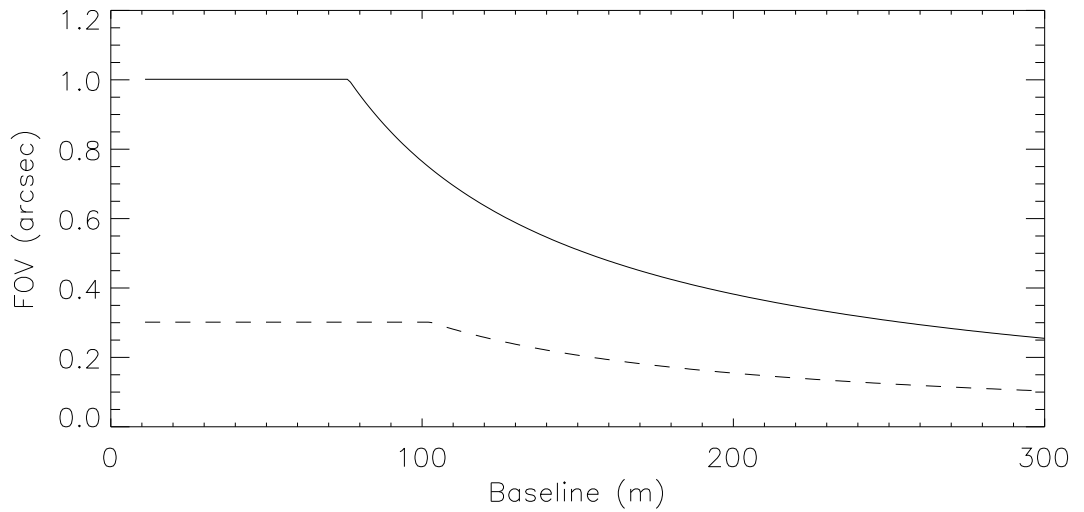


Figure 6: The field of view for the visible (dashed line) and IR (solid line) bands. For the smaller baselines the FOV is restricted by the Airy disk size while for the large baselines differential optical paths start to dominate.

observations in the visible and IR bands impossible. It would, however, be possible for one to use the $0.9\text{-}1.0\ \mu\text{m}$ band without dispersion correction for fringe tracking while studying in the IR band. The field of view of the instrument is restricted by the size of the Airy pattern on baselines of less than approximately 100 m and becomes smaller for larger baselines because of the optical path length difference that is introduced by the angular offset.

Acknowledgments

This work was supported by the Center for High Angular Resolution Astronomy at Georgia State University during the design phase for the CHARA Array. CHARA research has been funded by the National Science Foundation through NSF Cooperative Agreement AST90-08941.

References

- [1] H.A. McAlister, W.G. Bagnuolo, T.A. ten Brummelaar, W.I. Hartkopf, I.K. Furenlid, S.T. Ridgway, J.W. Beletic, A.K. Garrison & W.G. Robinson *The CHARA Array: Final Report to the National Science Foundation* (Report to NSF: Cooperative Agreement 90-08941, Atlanta, 1994)
- [2] H.A. McAlister, W.G. Bagnuolo, T.A. ten Brummelaar, W.I. Hartkopf, N.H. Turner, A.K. Garrison, W.G. Robinson & S.T. Ridgway, "The CHARA Array" in *Proc: SPIE conference on Advanced Telescopes & Instrumentation*, 2200 (1994), pp. 129-139.

- [3] L. Koechlin, “The I2T Interferometer ” in *Proc: NOAO/ESO Conference on High Resolution Imaging by Int.*, Ed: F. Merkle (1988), pp. 695-704.
- [4] F. Vakili, D. Bonneau, P. Lawson, G. Merlin, D. Mourard, P. Stee, I. Tallon-Bosc and F. Vallée, “Spectrally resolved interferometry with Grand Interféromètre à 2 Télescopes” in *Proc: SPIE conference on Advanced Telescopes & Instrumentation*, 2200 (1994), pp. 216-221.
- [5] J. Davis, W.J. Tango, A.J. Booth, R.A. Minard, S.M. Owens and R.R Shobbrook, “Progress in commissioning the Sydney University Stellar Interferometer (SUSI)” in *Proc: SPIE conference on Advanced Telescopes & Instrumentation*, 2200 (1994), pp. 231-241.
- [6] W.J. Tango, “Dispersion in Stellar Interferometry,” *Applied Optics*, **29**, 516-521 (1990)
- [7] W. Traub, “Visibility Loss with an Air Filled Delay Line,” IOTA Internal Report, (1990)
- [8] N.P. Carleton, W.A. Traub, M.C. Lacasse, P. Nisenson, M.R. Pearlman, R.D. Reasenberg, X. Xu, C. Coldwell, A. Panasyuk, J.A. Benson, C. Popaliolios, R. Predmore, F.P. Schloerb, H.M. Dyck & D. Gibson , “Current Status of the IOTA interferometer ” in *Proc: SPIE conference on Advanced Telescopes & Instrumentation*, 2200 (1994), pp. 152-165.
- [9] J.T. Armstrong, “Progress report on the BOA ” in *Proc: SPIE conference on Advanced Telescopes & Instrumentation*, 2200 (1994), pp. 62-70.
- [10] L. Ling, “Air Path Mismatch Compensation,” N.R.O. Tech Report, **OIPTR 90-001**, (1990)